Electrochimica Acta 56 (2011) 3981–3987

Contents lists available at ScienceDirect

Electrochimica Acta

journal homepage: www.elsevier.com/locate/electacta

Cyclability study of silicon–carbon composite anodes for lithium-ion batteries using electrochemical impedance spectroscopy

Juchen Guo[a], Ann Sun[a], Xilin Chen[a], Chunsheng Wang[a,*], Ayyakkannu Manivannan[b]

[a] Department of Chemical & Biomolecular Engineering, University of Maryland, College Park, MD 20742, United States
[b] US Department of Energy, National Energy Technology Laboratory, Morgantown, WV 26507, United States

ARTICLE INFO

Article history:
Received 13 December 2010
Received in revised form 4 February 2011
Accepted 4 February 2011
Available online 18 February 2011

Keywords:
Li-ion battery
Silicon anode
Cyclic stability
Carbon nanotube
Electrochemical impedance spectroscopy

ABSTRACT

The effects of carbonization process and carbon nanofiber/nanotube additives on the cycling stability of silicon–carbon composite anodes were investigated by monitoring the impedance evolution during charge/discharge cycles with electrochemical impedance spectroscopy (EIS). Three types of Si–C anodes were investigated: the first type consisted of Si nanoparticles incorporated into a network of carbon nanofibers (CNFs) and multi-walled carbon nanotubes (MWNTs), with annealed polymer binder. The second type of Si–C anodes was prepared by further heat treatment of the first Si–C anodes to carbonize the polymer binder. The third Si–C anode was as same as the second one except no CNFs and MWNTs being added. Impedance analysis revealed that the carbonization process stabilized the Si–C anode structure and decreased the charge transfer resistance, thus improving the cycling stability. On the other hand, although the MWNTs/CNFs additives could enhance the electronic conductivity of the Si–C anodes, the induced inhomogeneous structure decreased the integrity of the electrode, resulting in a poor long term cycling stability.

1. Introduction

Lithium-ion batteries have been recognized as an enabling energy storage technology for many emerging applications, including electric vehicles (EV) and plug-in hybrid electric vehicles (PHEV). However, the low specific capacity of commercially used graphite anodes is a limiting factor in the development of Li-ion batteries with high energy density. As a potential anode material, silicon stands out due to its superior theoretical specific capacity of 3579 mAh g^{-1} – the highest capacity of any known anode materials at room temperature [1] other than Li metal. However, Si-based anodes suffer from poor cycling stability due to severe Si expansion/shrinkage during Li insertion/extraction. Although the Si particle pulverization was alleviated by using Si nanoparticles or nanowires [2–4], the cyclic stability of nano-Si anodes still cannot satisfy the needs of practical applications due to the poor electrode structural stability during Li insertion/extraction cycles. To solve these problems, more attention has been recently paid on Si-based composite anode materials with improved structural integrity and electronic conductivity. Among them, Si–carbon composite anodes with carbon nano-materials, such as carbon nanotubes [5–11], graphene [12,13], and nano-porous framework structures [14–18] have demonstrated very promising performances. However, the mechanism behind the cyclability enhancement of Si anode composites with carbon nano-materials is still not fully understood due to a lack of a systematic study of the impedance (diffusion impedance, charge transfer impedance, solid electrolyte interface impedance, etc.) in Si–C anodes along charge/discharge cycles.

Electrochemical impedance spectroscopy (EIS) is a powerful electroanalytical technique for studying the kinetics occurring in the electrodes of Li-ion batteries. The resistance due to each kinetic step during the electrochemical reaction in the electrode can be obtained by EIS if the time constants are resolvable. Therefore, the evolution of the electrochemical and physical properties of the electrodes can be inferred from EIS data. The EIS technique has been used to investigate the lithiation/delithiation kinetics and structural evolution of the graphite electrodes [19–23]. Recently, EIS was also used to investigate the electrochemical behavior of some emerging electrode materials, including the lithiation kinetics of SnO and Sn [24,25], the formation of the solid electrolyte interface (SEI) on Si thin film electrodes [26], and the phase transformation and structural change of carbon-coated Si particles and Si nanowires [27–31]. These EIS studies mainly focused on the impedance change at different depths of discharge or charge in one specific cycle to investigate the reaction mechanism and kinetics during a lithiation or delithiation process. However, the poor cycling stability rather than kinetics is the major barrier for commercialization of high capacity Si–C anodes. Therefore, investigation of capacity decline mechanism of Si–C anodes by monitoring

---

* Corresponding author. Tel.: +1 301 405 0352; fax: +1 301 314 9126.
E-mail address: cswang@umd.edu (C. Wang).

0013-4686/$ – see front matter. Published by Elsevier Ltd.
doi:10.1016/j.electacta.2011.02.014

the evolution of the electrode impedances during the cycling process is of great importance for the development of an optimal Si–C electrode design. To the best of our knowledge, there is no study that has systematically investigated the impedance changes of the Si electrode during the entire cycling process especially, at the end of every discharged cycle.

For the first time, we used EIS to investigate the capacity decline mechanism of Si–C anodes by monitoring the impedance variation of electrodes as a function of cycle number. The obtained impedance data were interpreted by a model combining SEI resistance, charge transfer resistance, and interphase electronic contact resistance that represent the electrical contact between current collectors and electrode components, including Si nanoparticles, carbon additives, and binder. By combining and comparing the electrochemical performance tests and the EIS data, we attempted to acquire a better understanding of the mechanism behind the capacity fading of the Si–C electrodes.

Since the porous carbon frameworks from carbonization of polymer precursors and carbon nanotube/nanofiber additives are the most effective carbon materials to enhance the cycling stability of Si–C anodes, the effects of carbonization and multi-walled carbon nanotubes (MWNTs)/carbon nanofibers (CNFs) additives on the cycling stability were investigated by monitoring the impedance evolution of three types of Si–C electrodes (type 1: Si–MWNTs/CNFs with annealed polymer binder, type 2: Si–MWNTs/CNFs with carbonized polymer binder, and type 3: Si only with carbonized polymer binder). The influence of carbonization in cycling stability of Si–C anodes can be obtained by comparing the impedance difference between type 1 and type 2 electrodes during charge/discharge cycles, while the effect of addition of MWNTs/CNFs on cycling stability can be illustrated by the impedance difference between type 2 and type 3 electrodes. The characteristic dimensions of the employed CNF were 200–500 nm in diameter and 10–40 μm in length, and those of MWNT were 10–30 nm in diameter and 1–2 μm in length. This carbon network can improve the electronic conductivity of the electrode, because the network should be able to bridge Si active materials on both MWNT (small scale) and CNF (larger scale). The type 1 Si–C electrodes were annealed through heat-treatment at 250 °C (melting temperature of the polymer binder) in an inert gas environment. This heat–melt–cool process could redistribute the binder and form a more continuous binder phase, thus leading to better performance, as suggested by a previous study by Dahn et al. [32]. The type 2 Si–C electrodes were prepared by further heating the first type to 700 °C to carbonize the polymer binder, resulting in a porous carbon framework binder structure. The comparison of annealing process and carbonization process can be concluded from these two types of Si–C electrodes. The type 3 Si–C electrodes were prepared by mixing the Si nanoparticles and polymer binder without the CNFs/MWNTs additives, followed by carbonization at 700 °C.

2. Experimental

Silicon nanoparticles (20–30 nm), CNFs, and MWNTs were all purchased from Nano-structured & Amorphous Materials, Inc., and used as received. Polyacrylonitrile (PAN, molecular weight 150,000) was purchased from Sigma–Aldrich, and used as received. To prepare the first two types of Si–C electrodes, a mixture of Si nano-particles, CNFs, and MWNTs was blended in an 8 wt.% DMF (anhydrous, Sigma–Aldrich) solution of PAN. The composition of the resulting slurry was 40 wt.% Si nanoparticles, 15 wt.% CNFs, 5 wt.% MWNTs, and 40 wt.% PAN. The slurry was mixed for 1 h in an egg-shaped stainless steel vial using a Spex 8000 M mixer with zirconia balls as the milling media. The mixed slurry was cast onto a sheet of copper foil current collector and dried for 24 h in the fume hood, followed by drying overnight at 110 °C in a vacuum oven. The obtained Si–C electrodes were heated to 250° (PAN melting point) in a tube furnace for 3 h with flowing argon (Airgas, 95% Ar and 5% H_2) and then naturally cooled to room temperature to obtain the annealed electrodes. To obtain the carbonized electrodes, the electrodes described above were further heated from 250 °C to 700 °C and kept at 700 °C for another 3 h in the flowing argon environment. The heating rate for both steps was 5 °C min^{-1}. The third type of Si–C electrodes was similarly prepared without adding the MWNTs/CNFs, as described in details in a previous report [16].

Two-electrode coin half-cells with lithium foil as the counter electrode were assembled in an argon-filled glove box. Since EIS is sensitive to the loading of the Si active material, the Si loading of all electrodes was precisely controlled at 0.5 mg cm^{-2}. Electrolyte consisting of 1 M $LiPF_6$ in a mixture of ethylene carbonate and diethyl carbonate (1:1 by volume) was used with a micro-porous membrane separator (Celgard® 3501). The cells were discharged (Li-ion insertion) and charged (Li-ion extraction) with various cycling currents between 0.05 and 1.5 V (vs. Li/Li^+) using an Arbin™ battery test station. The EIS measurements were performed after the electrodes reached the end of discharge and relaxed until the open circuit potential reached 0.1 V. The measurements were taken over a series of cycles in a frequency range of 1000 kHz to 1 mHz with AC amplitude of 10 mV using a Solartron™ SI1287/1260 analyzer. The EIS data were fitted to the equivalent circuit using CorrWare® electrochemistry software to analyze the individual resistances. Thermogravimetric analysis (TGA) was carried out to determine the Si content in the carbonized electrodes using a thermogravimetric analyzer (Q50, TA instruments) with a heating rate of 5 °C min^{-1} in air. SEM images were taken using a Hitachi SU-70 Analytical Ultra-high Resolution scanning electron microscope.

3. Results and discussion

The SEM images of all three types of Si–C electrodes are shown in Fig. 1. The images of the annealed (Fig. 1a and b) and the carbonized electrodes (Fig. 1c and d) with MWNTs/CNFs clearly show the hierarchical carbon network. The structural difference between these two electrodes can be clearly distinguished: The components of the annealed Si–C electrode are bound by a continuous binder phase, as shown in the high magnification SEM image in Fig. 1b, while the carbonized Si–C electrode shown in Fig. 1d has a more porous structure, due to the carbonization of the PAN. Although the MWNTs/CNTs are uniformly distributed in the type 1 and type 2 Si–C electrodes (Fig. 1a–d), these additives may also induce local structural inhomogeneity, resulting in unevenly distributed local strain/stress in the electrode structure during the severe Si volume change, which may demolish the electronic connection between the Si active material and the conductive binder/additives. The structure of the third type of Si–C electrode is shown in Fig. 1e and f. The high magnification SEM in Fig. 1f shows a more homogenous porous structure without MWNTs/CNFs, comparing with the ones with MWNTs/CNFs.

The Si content in the annealed Si–C electrodes is 40 wt.% based on the composition in the electrode preparation. The Si contents in the carbonized electrodes were determined by the TGA analysis. The TGA results shown in Fig. 2 demonstrate that the carbonized Si–C electrode with MWNTs/CNFs contains 50 wt.% Si, and the one without MWNTs/CNFs contains 76 wt.% Si. The weight increase after 700 °C in the TGA curve is due to the oxidation of Si in air above 700 °C [33]. Based on the Si content before and after the carbonization, the weight loss of PAN during carbonization was estimated at 50 wt.%, which agrees with the reported value [34].

The reversible charge capacities over 120 cycles of these three Si–C electrodes are shown in Fig. 3 with the correspond-

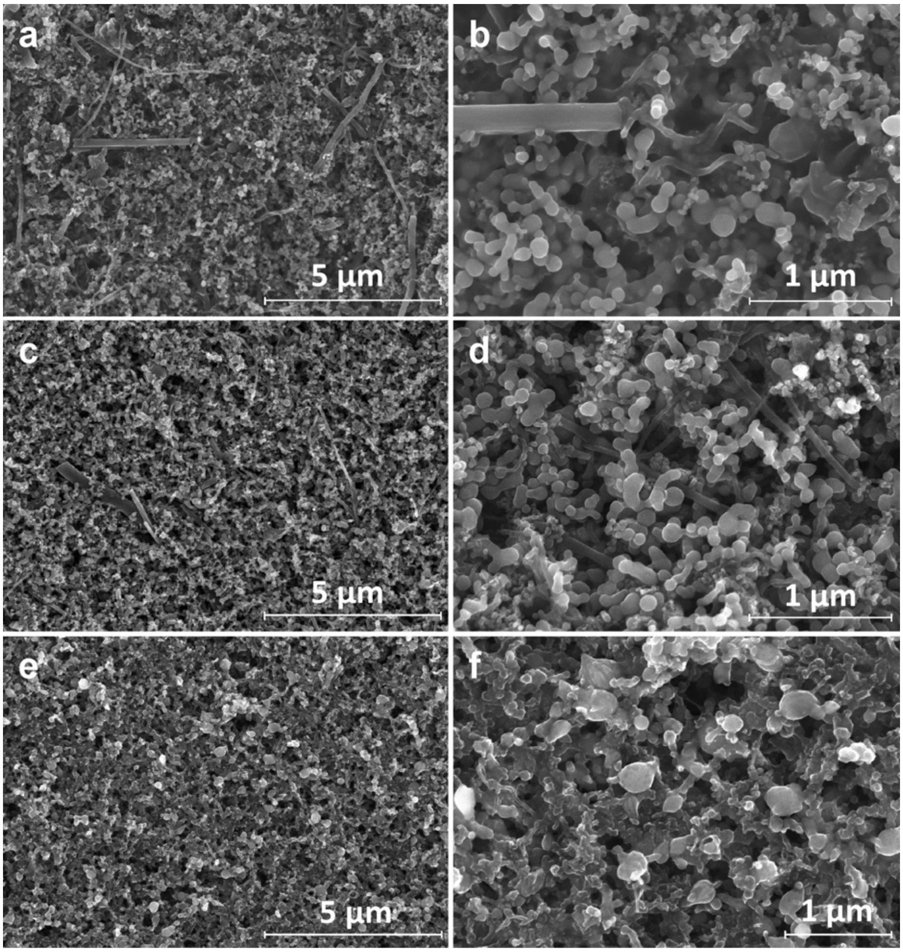

Fig. 1. SEM of (a) low magnification and (b) high magnification of the annealed Si–C electrode with CNFs/MWNTs; SEM of (c) low magnification and (d) high magnification of the carbonized Si–C electrode with CNFs/MWNTs; and SEM of (e) low magnification and (f) high magnification of the carbonized Si–C electrode without CNFs/MWNTs.

ing coulombic efficiency data. The discharge/charge current was 200 mA g^{-1} based on Si weight. The reversible charge capacities in the first cycle are 2300 mAh g^{-1} for the annealed electrode, 2750 mAh g^{-1} for the carbonized electrode with MWNTs/CNFs, and 2200 mAh g^{-1} for the carbonized electrode without MWNTs/CNFs. The capacity was calculated based on Si. The capacities of all three electrodes increased during the initial numbers of cycles, which will be discussed later. After reaching their peak values, the capacities of all electrodes decreased until the end of cycling. However, these cycling stability curves distinctly show that the capacity fading of the carbonized electrode without MWNTs/CNFs is much more mitigated comparing with the two electrodes with MWNTs/CNFs. As results, the reversible capacities after 120 cycles of the annealed Si–C electrode with MWNTs/CNFs, the carbonized Si–C electrode with MWNTs/CNFs, and the carbonized Si–C electrode without MWNTs/CNFs are 730 mAh g^{-1} (32% capacity retention), 1170 mAh g^{-1} (42% capacity retention), and 1550 mAh g^{-1} (70% capacity retention), respectively. Similarly,

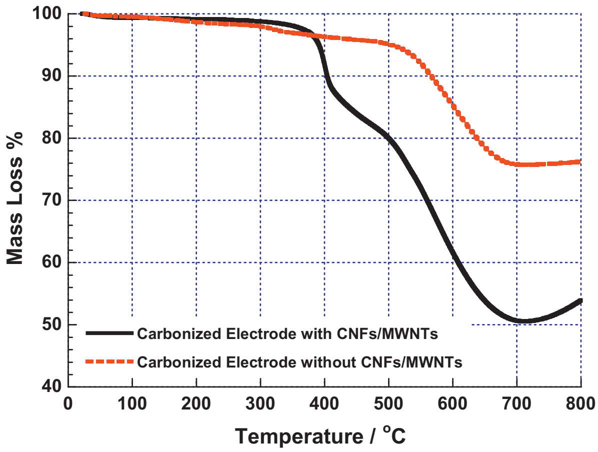

Fig. 2. TGA curve of the carbonized Si–C electrodes in air.

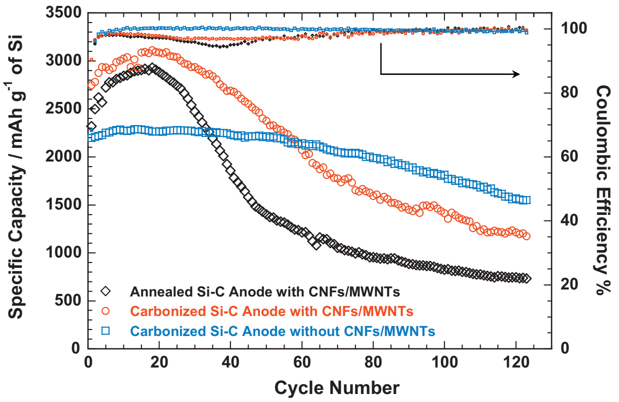

Fig. 3. Cyclability of the annealed Si–C electrode, the carbonized Si–C electrode with CNFs/MWNTs, and the carbonized Si–C electrode without CNFs/MWNTs under 200 mA g^{-1} charge/discharge current.

the coulombic efficiency curves of these three electrodes also show different patterns. The first cycle coulombic efficiencies of the annealed electrode, the carbonized electrode with MWNTs/CNFs, and the one without MWNTs/CNFs are 75.2%, 90.5% and 68.4%, respectively. The coulombic efficiency of the Si–C electrode without MWNTs/CNFs quickly increased to 100% after only a few cycles. On the contrary, the coulombic efficiencies of the other two electrodes with MWNTs/CNFs increased to 98% at the third cycle; and started to decrease until the 45th cycle and then increased gradually. Their coulombic efficiencies eventually reached 100% after about 80 cycles. It is interesting to note that the obvious dip in the coulombic efficiency curve of the annealed electrode accompanied its faster capacity fading, as indicated by the steeper capacity curve of the annealed electrode.

Comparing the cycling stability of the annealed Si–C electrode and the carbonized Si–C electrode, both with MWNTs/CNFs, the type 2 electrode has higher reversible capacity and better cyclability. The better cyclability can be clearly demonstrated by the less steep capacity decline of the carbonized electrode starting from the 20th cycle. The different cycling behaviors of type 1 and type 2 electrodes clearly show the performance improvement through the carbonization process. The cycling behaviors of the type 2 and 3 electrodes, both carbonized with and without MWNTs/CNFs, demonstrate that adding MWNTs/CNFs increase the electrode capacity in the early stage charge/discharge cycles, which is consistent with the reported results [11]. However, it has negative impact on the long term cycling stability of the Si–C electrodes as indicated by the inferior long-term cycling result of the type 2 Si–C electrode.

To better understand the capacity fading mechanism of these Si–C electrodes, EIS measurements were performed on the fully discharged electrodes. All measurements were taken after full relaxation, when the open circuit potentials of the electrodes reached 0.1 V. The Nyquist plots of the annealed Si–C electrode, the carbonized Si–C electrode with MWNTs/CNFs, and the carbonized Si–C electrode without MWNTs/CNFs at different charge/discharge cycles are shown in Figs. 4–6, respectively. As shown in Fig. 4, all the Nyquist plots of annealed Si–C electrode with MWNTs/CNFs are composed of two depressed semicircles in the high frequency (HF) region, one semicircle in the middle frequency region, and a sloped line in the low frequency region. The first semicircle with characteristic frequency of ~10^4 Hz can only be clearly observed by enlarging the HF region (inset of Fig. 4b). During the first 20 cycles, the magnitude of the second semicircle with characteristic frequency of 251 Hz rapidly decreases, while its characteristic frequency remains unchanged at 251 Hz during the decrease. It starts to slightly increase after the 45th cycle until the end of the cycling test (Fig. 4b). This observation suggests that the shrinking 251 Hz semicircles in sequential discharges actually reflect the impedance change of certain kinetic step. Meanwhile the third semicircle at a frequency of around 0.2 Hz keeps growing through the first 20 cycles. The Nyquist plots of the carbonized Si–C electrodes with MWNTs/CNFs and without MWNTs/CNFs exhibit similar behavior in Figs. 5 and 6. The difference in characteristic frequencies between type 2 and type 3 electrodes in Figs. 5 and 6 can be attributed to the MWNTs/CNFs additives.

Since two-electrode cells with Li metal counter electrode were used in the EIS measurement, the influence of the Li counter electrode has to be considered. Therefore, a symmetric cell with Li metal foil on both sides of the electrolyte was assembled and tested. The symmetric Li cell was charged and discharged for 5 h, respectively, using 0.1 mA cm^{-2} current. The impedance was measured after a series of cycles until a stable impedance spectrum was obtained. The obtained Nyquist plot of the symmetric Li cell is plotted in Fig. 7, where a depressed semicircle with a characteristic frequency of 310 Hz is observed. The impedance of the Li cell initially increases from the freshly made state and then decreases, finally stabilizes after 10 cycles, and remains similar impedance to 120 cycles. It can be estimated that the impedance due to the Li counter electrode is about 8 Ω (half of the final resistance shown in Fig. 7, since symmetric structure was used). Although the impedance of the Li counter electrode was included in the measured EIS of three Si–C anodes, a reliable impedance change of Si–C anodes can still be obtained after 10 charge/discharge cycles because the impedance of Li counter electrode became stable after 10 cycles.

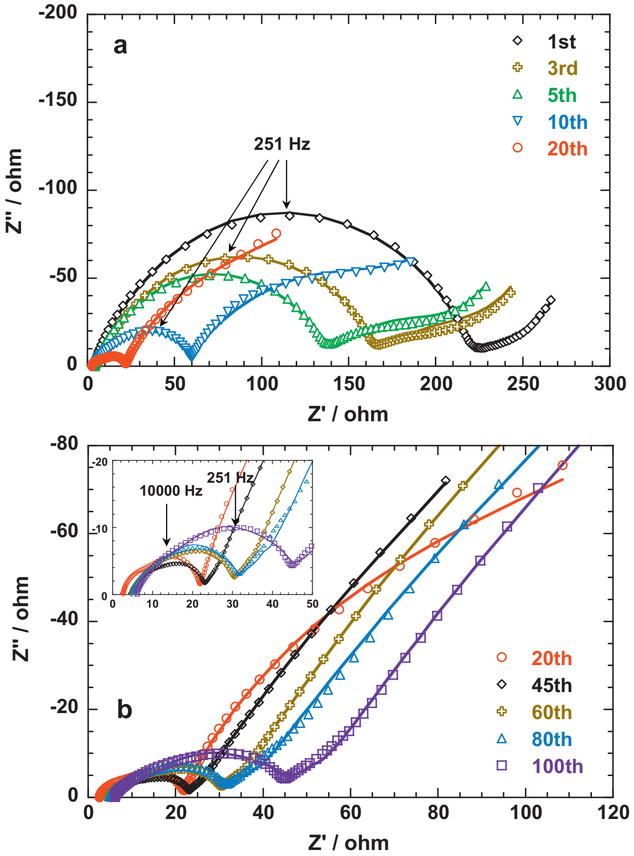

Fig. 4. Nyquist plots of the annealed Si–C electrode with CNFs/MWNTs after discharge in a series of cycles. Inset is the close-up of the high-frequency range.

The typical Nyquist plot of Li-ion battery electrodes consists of two semicircles and one 45° linear diffusion drift. The generally accepted interpretation of the Nyquist plot is that the HF semicircle is due to the formation of the SEI film, and the middle frequency semicircle is due to the impedance of the charge transfer reaction at the interface of electrolyte and active material. In this particular study, the third semicircle in the Si–C electrodes can be attributed to the charge transfer resistance. However, the two HF semicircles cannot be simply attributed to the SEI film resistance alone. A previous study on the HF impedance semicircles by Gaberscek and coworkers [35] suggested one of HF semicircle could be interpreted as the resistance of the interphase electronic contacts between the current collector and the conductive additive/binder system. Their experiments clearly demonstrated that increasing external load could significantly reduce the magnitude of the HF semicircle of the Nyquist plot of Li-ion battery electrodes. The behavior of our Si–C electrode EIS spectra is very much in agreement with the findings of Gaberscek et al. Moreover, the impedance modeling study by Dees et al. [36] also predicted that better interphase electronic contact could reduce the HF impedance semicircle. Based on the behavior of our EIS spectra and the aforementioned studies, we here propose an equivalent circuit for the Nyquist plots of our Si–C electrodes,

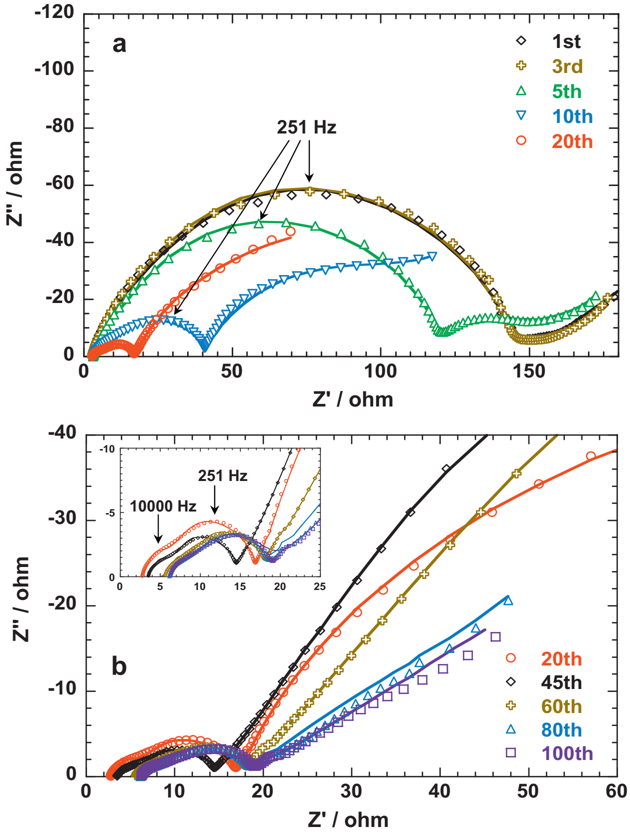

Fig. 5. Nyquist plots of the carbonized Si–C electrode with CNFs/MWNTs after discharge in a series of cycles. Inset is the close-up of the high-frequency range.

as shown in Fig. 8. This equivalent circuit consists of a series of three resistors and constant phase elements (CPE) in parallel and a Warburg diffusion element to account for the SEI film resistance (first HF semicircle), interphase electronic contact resistance (second HF semicircle) and charge transfer resistance (mid-frequency semicircle). The fitted impedances (solid lines in Figs. 4, 5 and 6) using this equivalent circuit agree well with the actual impedance data. By fitting the impedance data, the SEI resistance, interphase electronic contact resistance, and charge transfer resistance at different charge/discharge cycles were obtained. Fig. 9a is the SEI film resistance as a function of cycle numbers. The SEI resistances of the annealed and carbonized electrodes with MWNTs/CNFs start at similar level, and both exhibited fluctuations in a small range lower than 4 Ω in the first 10 cycles and then stabilized at 6 Ω for the annealed electrode and 2 Ω for the carbonized electrode after 30 cycles. The fluctuations of SEI resistance in the first 10 cycles may be attributed to the impedance interference from Li counter electrode. It is worth noting that the SEI resistance curve of the annealed electrode fluctuates between the 30th and the 70th cycle, which matches the coulombic efficiency curve dip of the annealed electrode shown in Fig. 3. The SEI resistance of the carbonized electrode without MWNTs/CNFs is stabilized at 17 Ω. The magnitudes of the SEI resistance, 6 Ω for the annealed electrode with MWNTs/CNFs, 2 Ω for the carbonized electrode with MWNTs/CNFs, and 17 Ω for the carbonized electrode without MWNTs/CNFs, are consistent with their initial irreversible capacities of 24.8%, 9.5%, and 31.6%, respectively. Fig. 9b is the interphase electronic contact resistance as a function of cycle numbers, which characterizes the direct electronic contact between the current collector and the additive/binder matrix combination. Unlike the SEI resistance, large decrease of interphase contact resistance was observed in all electrodes during the first 20 cycles, and then it slowly increased until the end of the cycling tests. The decrease of interphase electronic contact resistance can be attributed to the irreversible electrode volume increase during the first few Li insertion/extraction cycles [37,38]. Due to its continuously increased thickness, the Si–C electrode was pressed by a spring in the coin cell assembly, resulting in gradually increased pressure on the Si–C electrode. Therefore, the direct electronic contact between the current collector and the conductive additive/binder was improved, leading to decreased interphase electronic contact resistance. Furthermore, the more

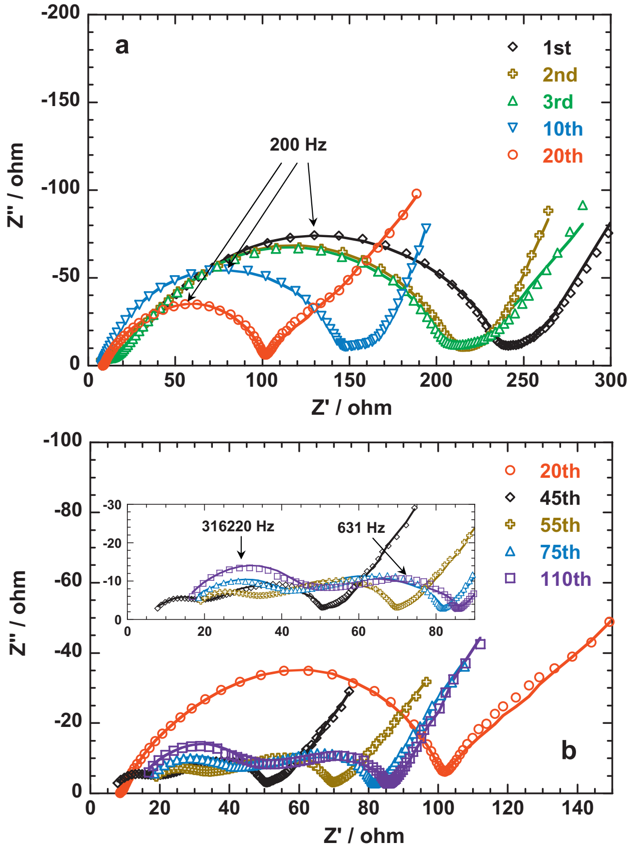

Fig. 6. Nyquist plots of the carbonized Si–C electrode without CNFs/MWNTs after discharge in a series of cycles. Inset is the close-up of the high-frequency range.

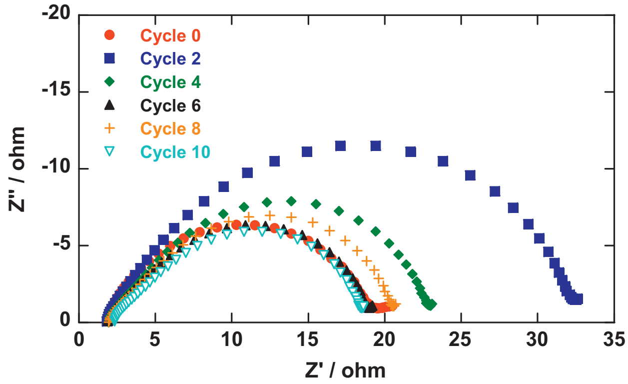

Fig. 7. Nyquist plots of the symmetric Li–Li cell of various cycles.

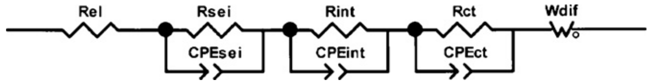

Fig. 8. The equivalent circuit used to model the impedance spectra in Figs. 4–6.

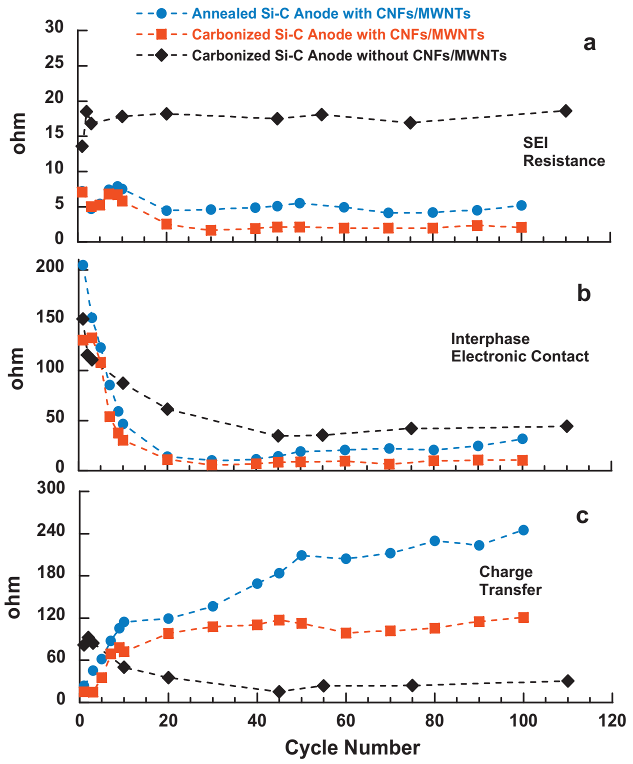

Fig. 9. Plots of (a) SEI film resistance, (b) interphase electronic contact resistance, and (c) charge transfer resistance as function of cycle number.

rapid decrease in the interphase contact resistance for the type 1 and 2 electrodes can be attributed to the high conductivity of MWNTs/CNFs.

Despite the consistent behaviors of all three electrodes in SEI resistance and interphase contact resistance, the charge transfer resistances (Fig. 9c) of these three indicate distinct difference. The charge transfer resistances of both electrodes with MWNTs/CNFs constantly increase during the cycling tests, and the increase is faster for the annealed electrode. On the contrary, the charge transfer resistant of the carbonized electrode without MWNTs/CNFs shows starkly different behavior: instead increasing, it decreases from a high initial value (82 Ω), reaching the lowest value (15.5 Ω) after 45 cycles, and then gradually and slightly increasing until the end of cycling. This difference may be explained by the following scenario: the charge transfer reaction takes place on the surface of the Si nanoparticles so that the direct electronic contact between the Si particles and the additive/binder has great influence on the charge transfer reaction. Comparing the electrodes with MWNTs/CNFs to the one without MWNTs/CNFs, their major difference is the addition of MWNTs/CNFs. Therefore, the increasing charge transfer resistance in the electrodes with MWNTs/CNFs can mainly be attributed to the demolition of electronic contact between Si nanoparticles and additives/binder due to the uneven local strain–stress distribution induced by the inhomogeneous electrode structure by adding MWNTs/CNFs. Also, the tortuosity of the electrode also plays an important role: some electrolyte flow channels in the electrode may be blocked by the structural demolition. It should be pointed out that the decreasing interphase contact resistance is not contradictory to the increasing charge transfer resistance in the electrodes with MWNTs/CNFs. The former one is induced by the tighter contact between the current collector and additive/binder system, and the later one is due to the weakened local contact between the Si nanoparticles and the conductive additives. Meanwhile, by sustaining good electronic contact between Si nanoparticles and conductive carbon framework, the charge transfer resistance in the carbonized electrode is improved. This capacity decline mechanism was well explained by Bruce et al. for porous β-MnO_2 cathodes of Li-ion batteries [39]. Addition of MWNTs/CNFs not only enhanced the conductivity of Si–C anodes, but also induced local structural inhomogeneous of the electrode structure, resulting in uneven stress/strain distribution in Si–C anodes during volume change of Si, which led to demolition of local electronic connections and block some electrolyte channels.

The sum of the increased charge transfer resistance and the decreased interphase contact resistance in the electrodes with MWNTs/CNFs in the first 20 cycles resulted in a decreasing net electrochemical impedance, which can explain the capacity increase in the first 20 cycles for both electrodes. The charge transfer resistance of the annealed electrode increased faster than that of the carbonized electrode, which led to its faster capacity fading. The increase in the charge transfer resistance of the carbonized electrode became much more moderate compared to that of the carbonized electrode after 50 cycles, and this eventually resulted in higher reversible capacity of the carbonized electrode. It suggests that the carbonized electrode has a more stable structure to preserve better connections between the Si nanoparticles and the conductive additives than the annealed electrode.

4. Conclusion

EIS technique has been used to investigate the impedance evolution of the porous Si–C composite electrodes during continuous charge/discharge cycles. This technique has been shown to be an effective tool to investigate the mechanism of cycling decline of porous Si–C anodes. The EIS study from three types of Si–C anodes (annealed and carbonized with MWNTs/CNFs, and carbonized without MWNTs/CNFs) demonstrated that the best performance of the carbonized electrode without MWNTs/CNFs can be attributed to a uniform porous carbon framework structure from the carbonization process. The structural homogeneity is of great importance for improving electrode cyclability, especially for porous Si electrode with high volume change during lithiation and delithiation.

Overall, electrodes with carbonized binder clearly have an advantage over ones using a conventional polymer binder, as they are able to provide better structural stability and connection between the Si active materials and conductive additives. Future investigations will be carried out to improve the electrochemical performance of Si electrodes through synthesizing homogenously structured carbon binder.

Acknowledgements

Financial support from the University of Maryland, College Park is gratefully acknowledged. We also acknowledge the support of the Maryland NanoCenter and its NispLab. The NispLab is supported in part by the National Science Foundation as a MRSEC Shared Experimental Facility.

References

[1] M.N. Obrovac, L. Christensen, Structural changes in silicon anodes during lithium insertion/extraction, Electrochem. Solid-State Lett. 7 (2004) A93–A96.
[2] C.K. Chan, H. Peng, G. Liu, K. Mclwrath, X.F. Zhang, R.A. Huggins, Y. Cui, High-performance lithium battery anodes using silicon nanowires, Nat. Nanotechnol. 3 (2008) 31–35.
[3] L.-F. Cui, Y. Yang, C.-M. Hsu, Y. Cui, Carbon–silicon core–shell nanowires as high capacity electrode for lithium ion batteries, Nano Lett. 9 (2009) 3370–3374.
[4] M.-H. Park, M.G. Kim, J. Joo, K. Kim, J. Kim, S. Ahn, Y. Cui, J. Cho, Silicon nanotube battery anodes, Nano Lett. 9 (2009) 3844–3847.
[5] J. Shu, H. Li, R. Yang, Y. Shi, X. Huang, Cage-like carbon nanotubes/Si composite as anode material for lithium ion batteries, Electrochem. Commun. 8 (2006) 51–54.

[6] B. Lestriez, S. Desaever, J. Danet, P. Moreau, D. Plee, D. Guyomard, Hierarchical and resilient conductive network of bridged carbon nanotubes and nanofibers for high-energy Si negative electrodes, Electrochem. Solid-State Lett. 12 (2009) A76–A80.

[7] J. Lee, J. Bae, J. Heo, I.T. Han, S.N. Cha, D.K. Kim, M. Yang, H.S. Han, W.S. Jeon, J. Chung, Effect of randomly networked carbon nanotubes in silicon-based anodes for lithium-ion batteries, J. Electrochem. Soc. 156 (2009) A905–A910.

[8] W. Wang, P.N. Kumta, Nanostructured hybrid silicon/carbon nanotube heterostructures: reversible high-capacity lithium-ion anodes, ACS Nano 4 (2010) 2233–2241.

[9] L.F. Cui, L. Hu, J. Wook, Y. Chi, Light-weight free-standing carbon nanotube-silicon film for anodes of lithium ion batteries, ACS Nano 7 (2010) 3671.

[10] Q. Si, K. Hansi, T. Ichikawa, A. Hirano, N. Imanishi, Y. Takeda, O. Yamamoto, A high performance silicon/carbon composite anode with carbon nanofiber for lithium-ion batteries, J. Power Sources 195 (2010) 1720.

[11] J.Y. Eom, J.W. Park, H.S. Kwon, S. Rajendran, Electrochemical insertion of lithium into multiwalled carbon nanotube/silicon composites produced by ballmilling, J. Electrochem. Soc. 153 (2006) A1678.

[12] J.K. Lee, K.B. Smith, C.M. Hayner, H.H. Kung, Silicon nanoparticles–graphene paper composites for Li ion battery anodes, Chem. Commun. 46 (2010) 2025–2027.

[13] S.-L. Chou, J.-Z. Wang, M. Choucair, H.-K. Liu, J.A. Stride, S.-X. Dou, Enhanced reversible lithium storage in a nanosize silicon/graphene composite, Electrochem. Commun. 12 (2010) 303–306.

[14] H. Kim, B. Han, J. Choo, J. Cho, Three-dimensional porous silicon particles for use in high-performance lithium secondary batteries, Angew. Chem. Int. Ed. 47 (2008) 10151–10154.

[15] P. Magasinki, B. Dixon, A. Hertzberg, J. Kvit, G. Ayala, Yushin, High performance lithium-ion anodes using a hierarchical bottom-up approach, Nat. Mater. 9 (2010) 353–358.

[16] J. Guo, X. Chen, C. Wang, Carbon scaffold structured silicon anodes for lithium-ion batteries, J. Mater. Chem. 10 (2010) 5035–5040.

[17] M. Li, M. Qu, X. He, Z. Yu, Electrochemical performance of Si/graphite/carbon composite electrode in mixed electrolytes containing LiBOB and LiPF6, J. Electrochem. Soc. 156 (2009) A294–298.

[18] J. Guo, A. Sun, C. Wang, A porous silicon–carbon anode with high overall capacity on carbon fiber current collector, Electrochem. Commun. 12 (2010) 981–984.

[19] Y.-C. Chang, H.-J. Sohn, Electrochemical impedance analysis for lithium ion intercalation into graphitized carbons, J. Electrochem. Soc. 147 (2000) 50–58.

[20] C. Wang, I. Kakwan, A.J. Appleby, F.E. Little, In situ investigation of electrochemical lithium intercalation into graphite powder, J. Electroanalyt. Chem. 489 (2000) 55–67.

[21] M. Umeda, K. Dokko, Y. Fujita, M. Mohamedi, I. Uchida, J.R. Selman, Electrochemical impedance study of Li-ion insertion into mesocarbon microbead single particle electrode Part I. Graphitized carbon, Electrochim. Acta 47 (2001) 885–890.

[22] S. Zhang, M.S. Ding, K. Xu, J. Allen, T.R. Jow, Understanding solid electrolyte interface film formation on graphite electrodes, Electrochem. Solid-State Lett. 4 (2001) A206–A208.

[23] J.Y. Song, H.H. Lee, Y.Y. Wang, C.C. Wan, Two- and three-electrode impedance spectroscopy of lithium-ion batteries, J. Power Sources 111 (2002) 255–276.

[24] H. Li, X. Huang, L. Chen, Electrochemical impedance spectroscopy study of SnO and nano-SnO anodes in lithium rechargeable batteries, J. Power Sources 81–82 (1999) 340–345.

[25] Z. Guo, Z. Zhao, H. Liu, S. Dou, Electrochemical lithiation and de-lithiation of MWNT–Sn/SnNi nanocomposites, Carbon 43 (2005) 1392–1399.

[26] Y.M. Lee, J.Y. Lee, H.-T. Shim, J.K. Lee, J.-K. Park, SEI layer formation on amorphous Si thin electrode during precycling, J. Electrochem. Soc. 154 (2007) A515–A519.

[27] N. Dimov, K. Fukuda, T. Umeno, S. Kugino, M. Yoshio, Characterization of carbon-coated silicon structural evolution and possible limitations, J. Power Sources 114 (2003) 88–95.

[28] N. Dimov, S. Kugino, M. Yoshio, Carbon-coated silicon as anode material for lithium ion batteries: advantages and limitations, Electrochim. Acta 48 (2003) 1579–1587.

[29] W. Liu, J. Wang, H. Wu, D. Shieh, M. Yang, N. Wu, Electrochemical characterizations on Si and C-coated Si particle electrodes for lithium-ion batteries, J. Electrochem. Soc. 152 (2005) A1719–A1725.

[30] Y.-M. Kang, J.-Y. Go, S.-M. Lee, W.-U. Choi, Impedance study on the correlation between phase transition and electrochemical degradation of Si-based materials, Electrochem. Commun. 9 (2007) 1276–1281.

[31] R. Ruffo, S.S. Hong, C.K. Chan, R.A. Huggins, Y. Cui, Impedance analysis of silicon nanowire lithium ion battery anodes, J. Phys. Chem. C 113 (2009) 11390–11398.

[32] J. Li, L. Christensen, M.N. Obrovac, K.C. Hewitt, J.R. Dahn, Effect of heat treatment on Si electrodes using polyvinylidene fluoride binder, J. Electrochem. Soc. 155 (2008) A234–A238.

[33] Y.-S. Hu, R. Demir-Cakan, M.-M. Titirici, J.-O. Muller, R. Schlogl, M. Antonietti, J. Maier, Superior storage performance of a Si@SiOx/C nanocomposite as anode material for lithium-ion batteries, Angew. Chem., Int. Ed. 47 (2008) 1645–1649.

[34] D. Hulicova, K. Hosoi, S. Kuroda, H. Abe, A. Oya, Carbon nanotubes prepared by spinning and carbonizing fine core–shell polymer microspheres, Adv. Mater. 14 (2002) 452–455.

[35] M. Gaberscek, J. Moskon, B. Erjavec, R. Dominko, J. Jamnik, The importance of interphase contacts in Li ion electrodes: the meaning of the high-frequency impedance arc, Electrochem. Solid-State Lett. 11 (2008) A170–A174.

[36] D. Dees, E. Gunen, D. Abraham, A. Jansen, J. Prakash, Alternating current impedance electrochemical modeling of lithium-ion positive electrodes, J. Electrochem. Soc. 152 (2005) A1409–A1417.

[37] B. Hertzberg, A. Alexeev, G. Yushin, Deformations in Si–Li anodes upon electrochemical alloying in nano-confined space, J. Am. Chem. Soc. 132 (2010) 8548–8549.

[38] U. Kasavajjula, C. Wang, A.J. Appleby, Nano- and bulk-silicon-based insertion anodes for lithium-ion secondary cells, J. Power Sources 163 (2007) 1003–1039.

[39] Y. Ren, A.R. Armstrong, F. Jiao, P.G. Bruce, Influence of size on the rate of mesoporous electrodes for lithium batteries, J. Am. Chem. Soc. 132 (2010) 996–1004.